TEMPORAL EVOLUTION OF A STREAMER COMPLEX: CORONAL AND IN SITU PLASMA PARAMETERS

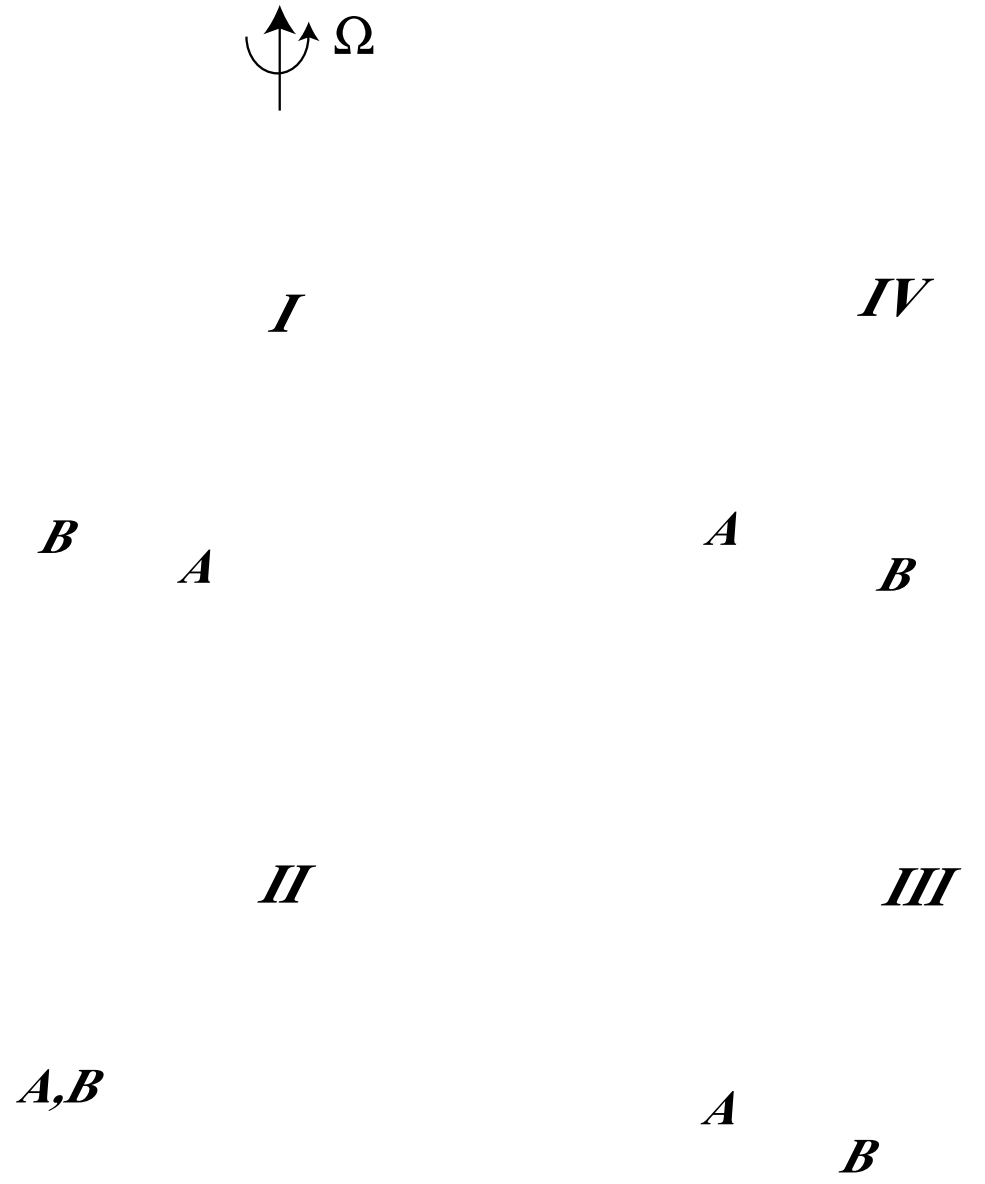

Fig. 2.—Cartoon representative of the scenario we described in the text for the behavior of the two streamers labeled A and B, rooted, respectively, on the back and front side of the Sun, as they are dragged around by solar rotation. The situation in the cartoon mimics what happens from June 12 through the following days. See Fig. 1 for a comparison with LASCO images.

acquired on June 10, 11, 12, 13, and 16 at an altitude of 1.6 R and on June 12, 13, 14, and 17 at an altitude of 1.9 R .

The strongest lines in the recorded spectral range are the H Ly and the O vi lines. Two sample spectra at two different grating positions are shown in Figure 4. Other ions, like Si xii, have emission 10 times lower than O vi lines, but they are still easily distinguishable. Total line intensities were computed by summing over all the bins along the line profile. The background level has been estimated from spectral intervals devoid of lines, and it has been subtracted from the line intensity.

For the strongest lines the calculated intensities have been compared with values derived from a Gaussian-plus-constant (or linear) background fit to the line. Values obtained from Gaussian fits and spectral integration agree within 5%. For the weakest lines the low statistics gave unreliable Gaussian fits, and intensities have been evaluated by summing over the line profile. The UVCS radiometric calibration has been made via the data analysis system (DAS), with an uncertainty of 20% for first-order lines and of 50% for second-order lines (Gardner et al. 2002). Corrections for stray light and flat-field effects have been made also using DAS before the line intensity was calculated.

To compare the spatial distribution of the UV line emission with white-light emission, we made plots of the total line intensity along the UVCS entrance slit. The position along the slit was converted to heliographic latitudes by simple geometric arguments. In the next figure (Fig. 5, *top*) we show LASCO C2 images for June 10 and 12 and (Fig. 5, *bottom*) the distribution along the UVCS slit of the line integrated intensity of the 1032 Å line of O vi and of the second-order Si xii line at 520.67 Å at 1.6 R . For a better statistics,

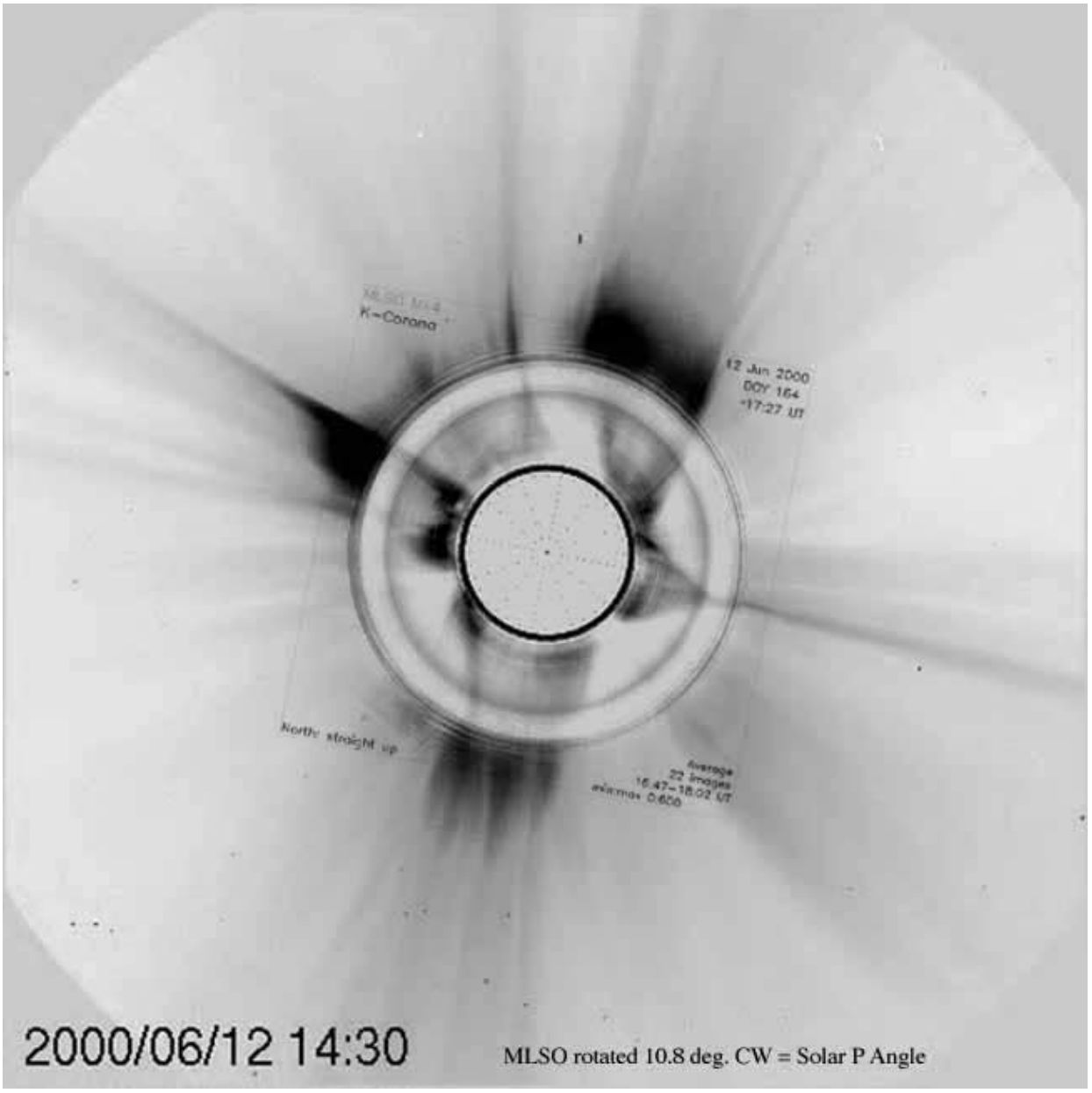

Fig. 3.—Composite image for 2000 June 12, showing the low corona from a Mauna Loa white-light image and, superposed, the outer corona from a LASCO C2 image. The figure shows that the LASCO C2 streamers in the southeast quadrant do not extend radially inward. The time at the bottom gives the time when the LASCO image was acquired; the Mauna Loa image is an average over 22 images taken between 16:47 and 18:02 UT.

UVCS data have been integrated over the whole time spent in each grating position; typically plots such as those given in the figure have been integrated over 2 hours. These lines originate from ions forming at quite different temperatures, as shown in Figure 6. In ionization equilibrium the O vi 1032 Å emissivity peaks at a temperature of 3 10^5 K, while the Si xii 520.67 emissivity peaks at a temperature of 2 10^6 K, with appreciable emission from plasmas at temperatures as high as 2 10^7 K.

As shown in Figure 5, on June 10, the O vi and Si xii intensities peak at the same latitude (48), at which the white-light emission is also brightest. This emission originates from the extension of streamer B^0 to the lower altitudes sampled by UVCS. The secondary O vi and Si xii intensity maxima originate from the extension to lower altitudes of streamer A (latitude of 70). However, on June 12, at the position of O vi maximum intensity, the Si xii emission is altogether negligible, while appreciable white-light and Si xii emission keeps originating from streamer A. Note that the shift in the location of the Si xii maximum from 70 (on June 10) to 60 (June 12) in latitude is due to solar rotation, which drags A, rooted on the back side of the Sun, to lower latitudes. Plots analogous to those given in Figure 5 allow us to follow the behavior of streamer A and B throughout the UVCS data set. The shift in the position of the UV streamers as they are carried around by solar rotation is consistent with the shift of the streamers in LASCO images. For the sake of simplicity, in the following we refer only to the centers of streamers A and B, rather than to the positions of maxima along the UVCS slit that identify them, because these change with time.

TABLE 1

Most Intense Lines Identified in the O vi Channel Spectral Range

λ_{obs} (Å)	λ_{ID} (Å)	Ion	Transition	log T_{max}[a]
972.51	972.54	H i	Ly	4.5
974.08	487.03	Fe xiii	$3s^2 3p^2\,{}^3P_2$–$3s\,3p^3\,{}^5S_1$	6.2
976.99	977.02	C iii	$2s^2\,{}^1S_0$–$2s\,2p\,{}^1P_1$	4.8
998.76	499.37	Si xii	$1s^2 2s\,{}^2S_{1/2}$–$1s^2 2p\,{}^2P_{3/2}$	6.3
1018.77	1018.60	Ar xii	$2s^2 2p^3\,{}^4S_{3/2}$–$2s^2 2\,p^3\,{}^2D_{5/2}$	6.3
1020.05	510.05	Fe xiii	$3s^2 3p^2\,{}^3P_2$–$3s\,3p^3\,{}^5S_2$	6.2
1025.69	1025.72	H i	Ly	4.5
1028.04	1028.04	Fe x	$3s^2 3p^4 3d\,{}^4D_{7/2}$–$3s^2 3\,p^4 3d\,{}^4F_{7/2}$	6.0
1031.90	1031.91	O vi	$1s^2 2s\,{}^2S_{1/2}$–$1s^2 2\,p\,{}^2P_{3/2}$	5.5
1034.50	1034.48	Ni xiv	$3s^2 3p^3\,{}^4S_{3/2}$–$3s^2 3p^3\,{}^2P_{3/2}$	6.2
1037.63	1037.61	O vi	$1s^2 2s\,{}^2S_{1/2}$–$1s^2 2\,p\,{}^2P_{1/2}$	5.5
1041.04	520.66	Si xii	$1s^2 2s\,{}^2S_{1/2}$–$1s^2 2\,p\,{}^2P_{1/2}$	6.3
1054.87	1054.90	Ar xii	$2s^2 2p^3\,{}^4S_{3/2}$–$2s^2 2p^3\,{}^2D_{3/2}$	6.3
1100.14	550.01	Al xi	$1s^2 2s\,{}^2S_{1/2}$–$1s^2 2p\,{}^2P_{3/2}$	6.2
1115.52	557.74	Ca x	$3s\,{}^2S_{1/2}$–$3p^2\,P_{3/2}$	5.8
1136.24	568.12	Al xi	$1s^2 2s\,{}^2S_{1/2}$–$1s^2 2p\,{}^2P_{1/2}$	6.2
1174.64	1174.65	Ni xiv	$3s^2 3p^3\,{}^4S_{3/2}$–$3s^2 3p^3\,{}^2P_{1/2}$	6.2
1196.11	1196.25	S x	$2p^3\,{}^4S_{3/2}$–$2p^3\,{}^2D_{5/2}$	6.1
1215.70	1215.67	H i	LyLy	

Unless there has been a dramatic drop in the abundance of Si in streamer B, the behavior shown in Figure 5 can be interpreted as an indication that streamer B is a cooler structure than streamer A, because it does not reach temperatures high enough to give rise to an appreciable emission in the Si xii 499 Å line. On the contrary, streamer A emission in Si xii is approximately constant over these 3 days. This qualitative analysis shows that different streamers may have different temperatures and that white-light images obviously are unable to convey any information in this respect. In x 4 we will show that the interpretation of the Si xii behavior in terms of a temperature rather than an abundance effect is correct.

The distribution of O vi and Si xii line intensity along the UVCS slit for the other days and for the height of 1.9 $R_\odot$ confirms the results obtained on June 12 and shown in Figure 5; that is, streamer B is still persistently "cold," with respect to streamer A. In the last days of our observational campaign, streamer B is off the UVCS field of view and streamer A occupies most of the UVCS slit. A plot of the intensity distribution of O vi and Si xii line intensity along the UVCS slit is shown in Figure 7

TABLE 2
Logarithm of Electron Temperatures for Streamers A and B

Date	Streamer	1.6 R		1.9 R	
2000 June 11.....	B	6.01	0.03	...	
2000 June 11.....	A	6.12	0.04	...	
2000 June 12.....	B	6.03	0.02	...	
2000 June 12.....	A	6.13	0.04	...	
2000 June 12.....	B	...		6.01	0.04
2000 June 12.....	A	...		6.14	0.06
2000 June 13.....	B	6.08	0.03	...	
2000 June 13.....	A	6.09	0.04	...	
2000 June 13.....	B	...		6.02	0.04
2000 June 13.....	A	...		6.15	0.06
2000 June 14.....	B	...		6.12	0.04
2000 June 14.....	A	...		6.14	0.06

streamer A is at the lowest temperature compatible with the uncertainty and that the low-temperature streamer B is at the highest temperature compatible with the uncertainty decreases the log T difference between A and B to 0.03–0.04, that is, to about a 10% difference. The reason a slight temperature variation has such a dramatic effect on the Si xii line visibility (see Fig. 5) lies in the shape of the ionization curve for Si xii (see Fig. 6). Between $\log T \approx 6.0$ and $\log T \approx 6.1$ the population of Si xii increases by a factor of 50. We will come back to this point when discussing the abundances in the streamers.

The temperatures of A and B compare favorably with previous estimates of temperatures in streamers. In particular, the temperature of streamer A agrees with the scale height temperature given by Gibson et al. (1999) for the WSM streamer at minimum of the activity cycle. Wilhelm et al. (2002) give a streamer temperature $T_e \approx 1.4 \times 10^6$ K at a heliocentric distance of 1.11 R in the rising phase of the activity cycle, which is compatible with our estimate, since temperature is supposed to increase and reach a maximum somewhere in between 1 and 1.5 R (Gibson et al. 1999). However, we did not find any evidence for plasma at $T_e \approx 2.2 \times 10^6$ K at 1.6 R, which Foley et al. (2002) found in streamers observed in 1999 August, close to solar maximum. The results of Foley et al. (2002) were based on an emission measure analysis of CDS data. In streamers at maximum these showed the presence of a much higher percentage of plasma, giving rise to emission in Fe xiii, Fe xiv, and Fe xv, than observed in streamers at minimum. In our data even Fe xiii is hardly identifiable. The reason for this discrepancy is not known. Possibly individual streamers at maximum activity cover a wider range of temperatures than at minimum, and Foley et al. structure belongs to a higher temperature class than streamers studied in the present work.

Data do not allow us to come to definite conclusions about the behavior of temperature with time. The temperature of streamer A is constant with time, in agreement with results from Li et al. (1998), who did not find any major variation in the physical parameters of streamers observed over a 6 day time span. The temperature of streamer B possibly increases slightly with time. Its temperature is lower than most of the estimates cited above. Whether this is related to the age of the streamer, for example, whether B is a newly formed structure that is slowly heating up, is an interesting hypothesis that should be checked on other streamers.

TABLE 3
Logarithm of Electron Temperatures across Streamer A

Date	Streamer	1.6 R		1.9 R	
2000 June 16.....	Center	6.15	0.03	...	
2000 June 16.....	Edge	6.08	0.04	...	
2000 June 17.....	Center	...		6.12	0.04
2000 June 17.....	Edge	...		6.07	0.0

4.1.2. *Electron Temperatures across a Streamer*

As we mentioned in § 2, we deem June 16/17 to be the time when A is seen against the plane of the sky. The profiles of the O vi 1032 Å and Si xii 520 Å line intensities along the UVCS slit for June 17, given in Figure 7 (*left*), may be compared with the LASCO C2 images for June 16 and 17 (UVCS data have been acquired between 7:45 UT of 2000 June 16 and 7:30 UT of 2000 June 17). The high-latitude portion of the streamer is seen to merge into the adjacent coronal hole without being hindered by any other structure. This allows us to derive the electron temperature distribution *across* the streamer.

To this end, we derived the electron temperature profile along the UVCS slit. This is given in Figure 7 (*right*). We caution the reader that values at high latitudes (that is, in the coronal hole area) are only tentative, because ionization equilibrium may not hold in a plasma outflowing region. Also, because only the center of the UVCS slit (bin 15 latitude 58) is at 1.6 R and its edges extend to higher altitudes, the variation of temperature with altitude affects the temperature profile. However, the plot points to a decrease of the electron temperature as we move from the center toward the edges of the streamer, in agreement with preliminary results obtained by Parenti et al. (2001). The temperature difference between the streamer peak and its (southern) edge, which we locate at the distance where the intensity drops by $1/e$ of the peak value, amounts to 0.05–0.06 dex, that is, is on the order of 10% to 15%. Table 3 gives temperatures at the center and at the edge of the streamer at 1.6 and 1.9 R. It is worth pointing out that this result refers to a streamer that does *not* show the weak oxygen emission core that has been found in UVCS images of streamers at the minimum phase of the activity cycle (see, e.g., Kohl et al. 1997).

4.2. *Densities in Streamers*

Once electron temperatures are known, we can make an evaluation of the electron density in streamers A and B from oxygen lines for a static streamer plasma, taking advantage of the N_e and N_e^2 dependence of, respectively, the line radiative and collisional components. Following Noci et al. (1987)

$$\frac{I_{12}}{I_{13}} = \frac{q_{1037} N_1 + 4\, j_{12}/h_{12}}{q_{1032} N_1 + 4\, j_{13}/h_{13}}\,; \qquad (1)$$

where I_{12} and I_{13} indicate, respectively, the intensities of the 1037 and 1032 Å lines of O vi; j_{12} and j_{13} are the emissivities of the resonantly scattered component of the lines; 1, 2, and 3 indicate, respectively, the ground, lower, and upper levels of the transition from which the doublet lines originate; N_1 is the population of the ground level; q_{1037} and q_{1032} are the collisional excitation rates from the ground level; and the

other symbols have their usual meaning. Equation (1) can be rewritten as

$$\frac{I_{12}}{I_{13}} = \frac{g_2}{g_3}\,\frac{1 + (g_2/g_3)}{1 + \eta} \quad ; \qquad (2)$$

with g the statistical weights of the levels and η, which represents the ratio between the collisional and radiative component of the 1032 line, given by

$$= 5{:}75 \quad 10^2$$

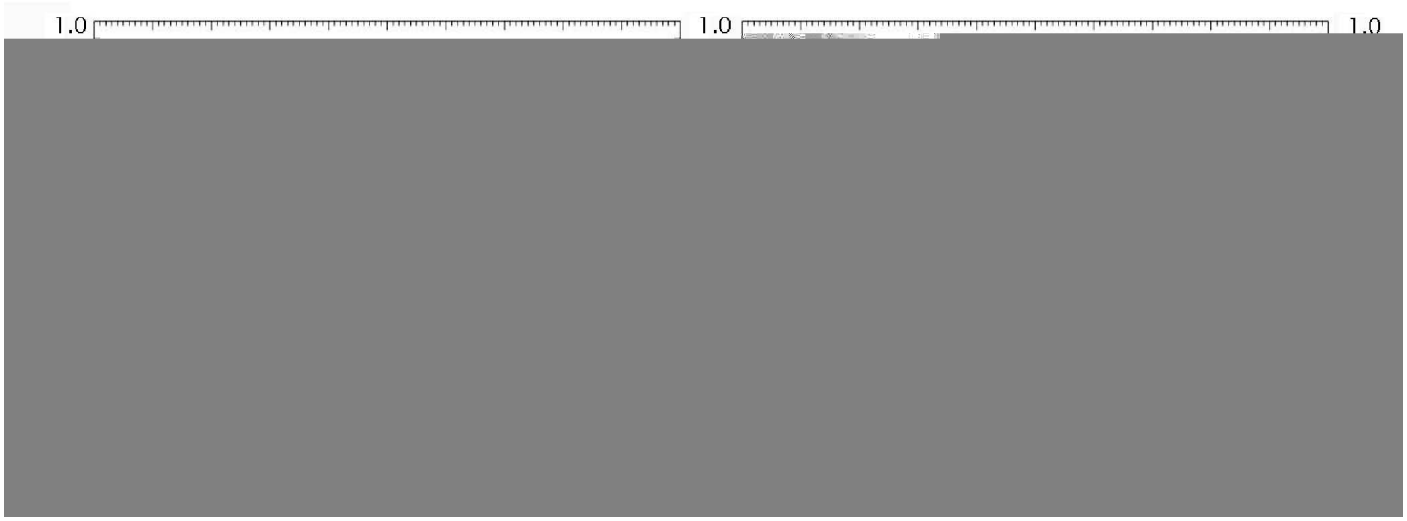

Fig. 10.—*Left*, Coronal element abundances (logarithm, with respect to photospheric values) against their FIP values for 2000 June 11 data at 1.6 R for streamer A (*diamonds*) and B (*asterisks*); *right*, same as for the left, but for 2000 June 12. The dotted lines correspond to a FIP bias of 4.

There are not many measurements of the FIP effect in streamers (see, e.g., Feldman et al. 1998), and often results are contradictory (see, e.g., Schmelz 1999). Moreover, they refer to lower altitudes than examined here. At heliocentric distances comparable to ours, however, Raymond (1999) found a behavior similar to that shown by streamer A in the core of the streamers he analyzed and a behavior similar to that shown by streamer B in active regions and/or legs of streamers. In the scenario we have been pursuing so far, an explanation for the observed behavior calls for a FIP effect imposed at chromospheric levels, with gravitational settling afterward modifying the values of the abundance ratios, but not the FIP bias. As we said, possibly conditions in "young" streamer B have not been stable long enough for gravitational settling to reduce the abundances of low-FIP elements, which, on the contrary, are depleted in the "older" streamer A. A similar explanation has been given by Raymond (1999) to interpret the difference between the abundances in the core of streamers and the abundances in active-region streamers.

5. ABUNDANCES MEASURED IN SITU AND THEIR CORONAL COUNTERPARTS

During the JOP 112 campaign, *Ulysses* was at a southern latitude of 58 , as mentioned. In spite of this rather high latitude, because of the phase of the activity cycle, *Ulysses* was immersed in slow wind. SWICS data show that the solar wind speed emanating from the Sun between 2000 June 10 and 17 was about 350 km s ^{1}, which is typical of the slow wind originating from noncoronal hole areas (see Fig. 11, *top*); hence, we expect in situ abundances to show a FIP effect on the order of 2–3 in contrast to high-speed wind for which the FIP effect is negligible (see, e.g., Geiss 1998; Von Steiger et al. 2000, 2001). This behavior is consistent with the FIP pattern in the corona, weak FIP effect having been found in coronal holes (Feldman & Widing 1993; Doschek et al. 1998; Doschek & Laming 2000), from which fast wind originates. Quadrature configurations allow us to make a direct comparison between the coronal FIP and the in situ FIP effect. Because the abundances of only a few elements are measured in situ, we chose the Fe/O abundance ratio as a proxy for the FIP bias, both elements being prominent among, respectively, the low/high FIP elements.

Because UVCS data have been acquired below the altitude at which the magnetic field is radial, we need first to extrapolate the photospheric magnetic field out to the altitude at which the field is radial, reconstructing a map of the field configuration at coronal levels. Then we locate the position of the *Ulysses* footpoint on this map and identify along the UVCS slit the location of the plasma that eventually reaches *Ulysses*. To do this, we utilize the MHD model of the corona and inner heliosphere described in Riley, Linker, & Mikić (2001). This model uses the observed line-of-sight component of the magnetic field as the inner boundary condition for a fully three-dimensional MHD model of the corona. Ideally, this model would allow mapping the *Ulysses* data back to the Sun by using the inverse MHD technique. However, the solar magnetic field was changing relatively rapidly at the time of JOP 112, so this is not possible. Instead we extrapolated the photospheric magnetic field measured at the Wilcox Solar Observatory to coronal altitudes and made magnetic field maps at several heights. These maps allowed us to infer the location of the footpoint of *Ulysses* with respect to the neutral line. From this we have been able to determine which side of the streamer observed by UVCS has been the source of the in situ measurements. The shape of the streamers correlate well with those observed by LASCO.

The photospheric field used in the model and the predicted field at 1.6 R are shown in Figure 11 (for the projection of *Ulysses* footpoint at 1.6 R , see next paragraph). Region A in this figure is the mixed photospheric polarity region that gave rise to the band of streamers lying on the limb and containing streamers A and B discussed above. Region B in this figure was the source of the higher speed wind that followed the band of streamers. As might be expected at this phase of the solar activity cycle, the photospheric field has a complex pattern, which simplifies at coronal levels in part because short length scale variations are lost in the extrapolation into the corona, but also because short-timescale variations are lost in the smoothing used to estimate the field over the entire photosphere for a full solar rotation. In Figure 11 it is clear that *Ulysses* skims along the

neutral line for most of the JOP 112 campaign. From the model coronal configuration, we estimated the latitude and hence the position along the UVCS slit where field lines reaching *Ulysses* intersect the UVCS slit.

Values of Fe/O at these positions and the average Fe/O values measured by SWICS are given in Table 10. Among those we used there is only one UVCS grating position that